

SPIE/IS&T

International

Technical

Group

Newsletter

Electronic Imaging

Uniformity and modeling of color spaces

A color appearance model is composed primarily of adaptation transforms and a method to predict color-appearance attributes. Adaptation transforms predict corresponding colors and can model chromatic adaptation, luminance adaptation, and changes in viewing conditions. Appearance attributes are descriptions of color perception, i.e. lightness, chroma, hue, brightness, colorfulness unique hues, etc. Additionally, color appearance spaces may attempt to predict various color appearance phenomena such as the Hunt effect or the Abney effect. It should be noted that a color space that accurately predicts appearance attributes may not accurately predict small color differences equally throughout the space, especially near the neutral colors.

There has been significant attention paid to various appearance attributes over the past several decades. Recently, interest in hue uniformity has grown because of its importance when applied to gamut mapping. The work we recently presented¹ centered around finding surfaces of constant perceived hue. This work was a more comprehensive and statistically significant follow-on to Hung and Berns' 1995 experiment² to find loci of constant hue using a CRT display. The results showed that none of the popular color-appearance spaces (including CIELAB, CIELUV, Hunt, Nayatani, CIECAM97s) had a hue angle metric that was acceptably uniform. Indeed, a surface of constant metric hue in CIELAB exhibits a color

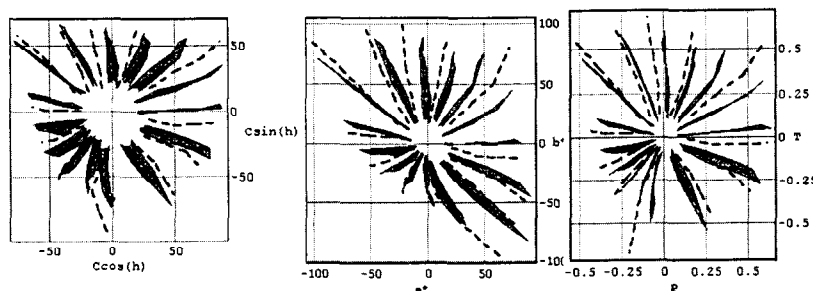


Figure 1. Constant hue surfaces in three color spaces. Dotted lines show Hung and Berns data, surface projections are from Ebner and Fairchild. CIECAM97s is on left, CIELAB is in the middle, and IPT is on the right.

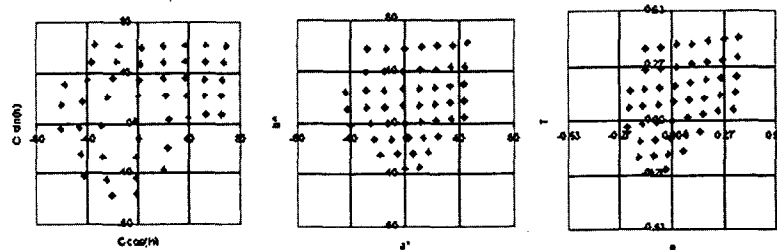


Figure 2. OSA uniform color scale at lightness of 0 in three color spaces. CIECAM97s is on left, CIELAB is in the middle, and IPT is on the right.

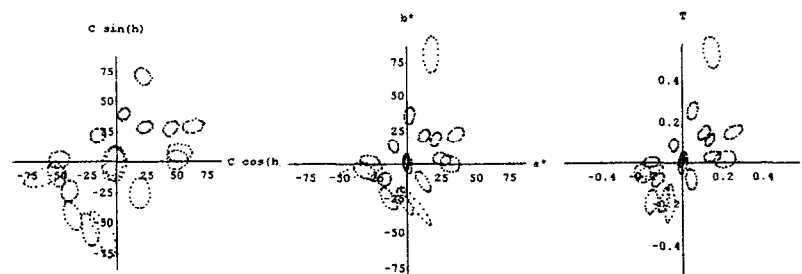


Figure 3. Suprathreshold color difference data in three color spaces. CIECAM97s is on left, CIELAB is in the middle, and IPT is on the right.

name change from purple to blue at a hue angle of 300°. Such appears to be the case with CIELUV and CIECAM97s as well, based on quantitative data.

It is desirable to employ a color space model

that is as simple as possible, both from a practical standpoint and because it may be more easily linked to fundamental properties of color vision. Additionally, a color space must be invertible in order to be feasible in image processing applications. Based on these design tenets, and from psychophysical data sets including the constant hue data sets described above, work was initiated to design a simple, invertible, more-uniform color space. After several unsuccessful attempts to solve the problem numerically, a technique was designed that allowed visualization of simple color space models. The technique allows the visual data sets to be transformed from fundamental tristimulus values through the color space model, with the results viewed on a CRT monitor. Free parameters of the color space can be altered and the resultant uniformity viewed in real time. Several color spaces were built from a color space visualization software program, and one was chosen that has the best overall uniformity.

Figures 1-3 show the results of the new color space (named IPT) compared to CIELAB, and CIECAM97s. Figure 1 shows that IPT is much more uniform in the hue

continued on p. 2

Editorial

Electronic imaging for digital publishing

It is time to reconsider our research priorities. The veterans in our community started out in an age when the image processing tools in the publishing industry were graphic arts cameras and screens, pin registers, knives, and goldenrod paper. Their contribution was to invent the technologies that brought us from mechanical processes to electronic publishing: scanners, image enhancement, colorimetric color control, color management, perceptually lossless image compression, and digital halftoning, among others.

It is a sign of the exponential progress in science and technology that the same generation of scientists and engineers is able to contribute to a new paradigm shift, namely from electronic publishing to digital publishing.

Digital publishing is a fully digital process, from end to end: cameras, scanners, processing, storage, syndication, distribution, and rendering. Many underlying electronic imaging technologies remain the same. However, the new fully-digital process changes the emphasis of which goals are more important, i.e., it requires us to reconsider the priorities of our research programs and objectives. One example is printer resolution.

The modulation transfer function (MTF) of today's printers is better than that of the human visual system. Concomitantly, the considerable image quality improvement in one-hour photo finishing processors has increased

user expectations. Consequently, the careful design of color-savvy halftoning algorithms has become much more critical, and it is no longer possible to apply the same grayscale algorithm to each color plane. With increased image sharpness, color artifacts are also more visible and color matching must be more accurate.

Only a few years ago, printer MTF was so poor that images could be aggressively compressed using the example quantization tables from the JPEG standard specification. Today, the quantization tables in lossy data-compression algorithms must be designed very carefully to be perceptually lossless for the intended rendering devices and viewing conditions.

The increased use of images in documents also poses new problems for our choice of data-compression-algorithm classes for images. While JPEG and wavelets work well on full-color images communicated over the internet, these algorithms fail on halftoned images. The last cable to the printer has become a severe performance bottleneck, and we need lossless compression methods like JBIG that do not destroy the structure of halftones.

I have touched on some components of a digital publishing system, and I shall finish on the glue that holds it all together, namely workflow. As images progress from creator to viewer, the electronic imaging algorithms must be able to operate in a pipeline. There is agreement on device profiles (although the imple-

mentations are still nightmares for users), file formats, communication protocols, and markup languages. However, other issues, such as end-to-end MTF optimization, color spaces, and rendering intent, are still open.

When we design electronic imaging algorithms for digital publishing systems, we should not forget that some of our technologies are taking a large human toll. Our new technologies are the basis for tools allowing everyone to do their digital publications by themselves. The pre-press industry, which worldwide employs an amazing number of imaging experts working in small businesses, is on the verge of disappearance. While mechanical paste-up assembly and stripping have gone the way of the buggy whip trade, we should not waste the specific knowledge in the pre-press industry. These talents are very much needed in the new world of digital publishing, especially now that we have to reconsider our research priorities. For example, a trained eye can take us a long way in end-to-end MTF optimization and choosing the most appropriate compression algorithms.

Giordano Beretta
Hewlett-Packard
1501 Page Mill Road 3U-3
Palo Alto, CA 94304
E-mail: beretta@hpl.hp.com

Uniformity and modeling

continued from cover

attribute of appearance than either of the other color spaces.^{1,2} This is the primary focus of improvement, so it was the most critical uniformity constraint. Figure 2 shows chroma uniformity³ using the OSA uniform color scale data at lightness 0. Notice that CIECAM97s has significantly larger differences in chroma distances near neutral colors. This is due to the nonlinear compression step applied to the chroma value. As is seen in figure 3, this chroma compression enables CIECAM97s to have more uniform color difference ellipses for small color differences.⁴ The data shown in figure 3 shows equal suprathreshold color differences for colors around 1 Delta E*ab. This points to a fundamental difference between large and small color-distance perception. As such, it may be appropriate to have separate models to predict the two phenomena.

The new color space (IPT) has a neutral lightness response that is nearly identical to the RLAB model, which is also quite close to that of the

CIELAB model. The lightness response of chromatic colors is more uniform and less dependent on hue region than that of CIELAB. A verification experiment was conducted that showed that the IPT color space was judged to be as uniform as hue-corrected color spaces (using look-up tables) based on both Hung and Berns', and Ebner and Fairchild's constant hue data sets. These results are more fully described in the conference proceedings of the IS&T/SID's 1998 color imaging conference held in November.

The most obvious application of a color space with improved hue uniformity is gamut mapping. The gamut volume of a common CRT computer display is much larger than that of most 4-color printers, especially in the blue region of color space. With the IPT color space, constant perceived hue gamut mapping can be done by simply constraining the metric hue to be constant. Preliminary results of applying the IPT color space for gamut mapping with color

laser printers is promising. Additional experiments are planned to further explore the properties of the IPT color space.

Fritz Ebner
Xerox Corporation
Bldg. 111-02j
Webster, NY 14580
E-mail: fritz.ebner@usa.xerox.com

References

1. Ebner and Fairchild, *Finding constant hue surfaces in color space*. *Proc. SPIE 3300*, p. 107, January 1998.
2. Hung and Berns, *Determination of constant hue loci for a CRT gamut and their predictions using color appearance spaces*. *Col. Res. & Appl.* **20** (5), p. 285, 1995.
3. Wyszecki and Stiles, *Color Science*, Second Edition, Wiley, ISBN 0-471-02106-7, p. 309, 1982.
4. Melgosa, Hita, Poza, Alman, and Berns, *Suprathreshold Color-Difference Ellipsoids for Surface Colors*. *Col. Res. & Appl.* **22** (3), p. 148, 1997.



Error diffusion with homogenous distribution in highlight and shadow regions

Error diffusion is a popular halftoning technique used to render continuous images on media with few output levels. It is applied mostly in printing, displaying or transmission. Essentially, the error diffusion process computes the difference between the input grayscale value of a pixel and its quantized output value, and selectively "diffuses" this difference, or error, to the neighboring unprocessed pixels of the input image. The error diffusion creates pleasant dot distributions for middle tone, but can lead to certain artifacts in shadow and highlight regions. Here, the dot distribution is loose and the eye is sensitive to the dot arrangement (the term "dot" identifies a white pixel in a shadow region, or a black pixel in a highlight region). Often, series of dots are perceived as "worms," rather than an input gray level (see figure 1).

Various methods have been proposed to reduce or eliminate "worm" artifacts.¹ Examples include threshold modulation (with noise, or a dither or imprint function), serpentine, changing the weighting mask (size, weighting values) or constraining the dots to certain positions.

We present here a technique that generates uniform dot distribution in highlight and shadow areas, introducing spatial constraints in the dot placement depending on the input gray level to be represented. For dots in the shadow or highlight regions, the spatial constraints inhibit the

dot pixels from being arranged in "worm" patterns. The proposed procedure can be seen as an implementation of the feedback error diffusion method proposed by Levien.²

The algorithm first determines whether the current pixel being processed is within the shadow or highlight region of the image. If so, a dot is placed in this region only if a distance constraint between the current position and neighboring dots is satisfied. If the distance constraint is not satisfied, the placement of the dot is postponed, and the corresponding error is diffused to the neighbor pixels in a conventional manner. The spatial constraint is based upon the original grayscale level of the current pixel. As the grayscale level to be represented approaches the limits of the grayscale range (e.g. 0 or 255 for 8 bits grayscale range), the minimum distance between dots increases. The minimum distance between each neighbor location and the current location can be directly calculated.

An alternate approach is a roadmap, or a path, that always starts at the current pixel position and expands further from the current pixel as its grayscale level approaches the extreme limits of the grayscale range. This path can be pre-calculated and stored in a lookup table, thereby providing a more efficient and less computationally intensive approach to ex-

amining the neighboring pixels for the distance constraint. The implementation uses two lookup tables (LUTs) as seen in figure 2. The first LUT provides the length of the roadmap covering the current pixel vicinity that should be investigated for the placement of dots. If at least one dot is found in this vicinity, the placement of the current dot is postponed. The second LUT stores the relative coordinates of each neighbor. These coordinates are always indexed from zero to the roadmap length value, extracted from the first LUT. The result of the proposed method displays a uniform dot distribution in highlight and shadow regions (figure 3). The proposed procedure can also be used for multi-level error diffusion.

Dr. Gabriel Marcu

Apple Computer, Inc.
1 Infinite Loop, MS: 82-CS
Cupertino, CA, 95014
E-mail: marcu@apple.com

References

1. Eschbach R., *Recent Progress in Digital Halftoning*, IS&T, 1994.
2. R. Levien, *Output dependent feedback in error diffusion halftoning*, Proc. IS&T's 46th Annual Conf. (Cambridge, MA), pp.115-118, 1993.



Figure 1. Worm artifacts in error diffusion.

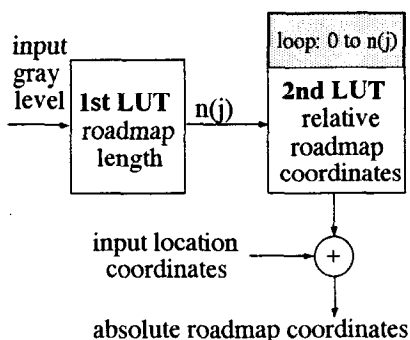


Figure 2. Block diagram of the algorithm.

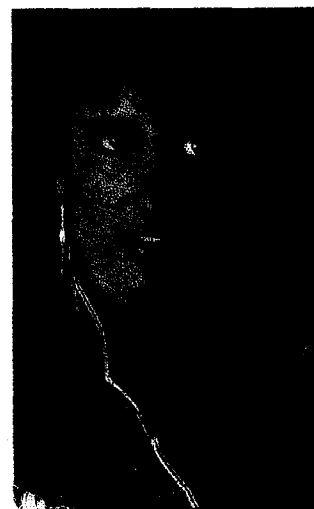


Figure 3. Result of proposed method.

Voronoi-based void and cluster algorithm

Continuous-tone images can be rendered on bi-level or multi-level devices by a process known as halftoning. Efficient and visually pleasing halftoning schemes based on pixel-wise thresholding decisions can be designed using frequency modulated (FM) screening. Some of the popular FM screening techniques are void and cluster,¹ and blue noise mask.²

FM screening methods construct an array of threshold values known as a dither array. To halftone a continuous tone image, the dither array is first tiled periodically to cover the image to be halftoned. Each pixel in the image is then compared to the corresponding threshold value from the dither array to decide whether a dot will be placed at that location. FM screens have high frequency noise characteristics and are pleasing to the human visual system. The problem, however, with using a single dither array is that if a dot is turned on at a particular location in a light tone, it will continue to be on in all darker tones. Thus, injudicious placement of dots in light tones may lead to disturbing halftoning artifacts in darker tones.

The methods developed in our work are derived from the void-and-cluster algorithm¹ for bitonal FM screening. The void and cluster method starts with a homogeneous initial binary-dot pattern. Dot patterns for lighter tones are generated by removing dots sequentially from the tightest clusters of dots in the current dot pattern. Similarly, adding dots sequentially to occupy the largest voids in the current dot pattern generates darker tones. Candidate locations for adding or removing dots in the binary patterns are determined by examining the response of fixed-width filters applied to the current binary pattern. All the locations in the dither array are ranked based on the order of dot placement in the binary pattern to generate the complete range of tones. The resulting array of ranks is quantized to yield a dither array of threshold values. The traditional algorithm however, does not have a strategy for selecting among candidates that have the same filter response. The lack of such a strategy leads to the selection either of the first candidate, or of a random selection among candidates. Both strategies may lead to non-uniform dot patterns that are especially disturbing in light and mid tones.

The void-and-cluster algorithm can be improved in terms of dot placement in light and dark tones by incorporating the following modi-

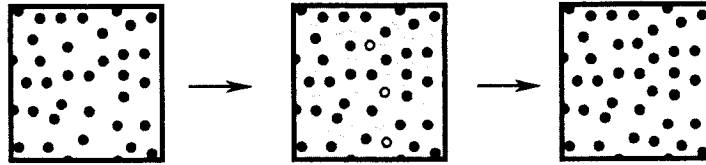


Figure 1. Voronoi-based void operation.

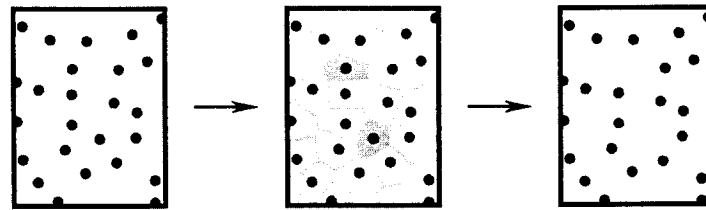


Figure 2. Voronoi-based cluster operation.

rent gray level into Voronoi regions.³ The Voronoi vertices represent candidates for the location of the largest void, while the Voronoi regions are used to determine the location of the tightest cluster. The largest void locations are identified by examining the response of Gaussian filter kernels centered at each Voronoi vertex. Removal and addition of dots using Voronoi-based clustering and void operations are illustrated in figures 1 and 2. The procedure is repeated until all array locations have been ranked.

When equally likely candidate locations are identified dur-

ing a void or cluster iteration, additional criteria are used to determine the best candidate.⁴ The first criterion improves spatial distribution of dots within a quantization level by examining distances to other dots that have been turned on in the same quantization level. If the first criterion does not resolve the degeneracy, the binary pattern is partitioned into blocks and a dot is added or removed so as to maintain the same dot density in each block. If both criteria fail to determine a unique candidate, the candidate is selected randomly.

The power spectra in figure 3 show an example of the improvement in dot distribution over the standard void and cluster method.

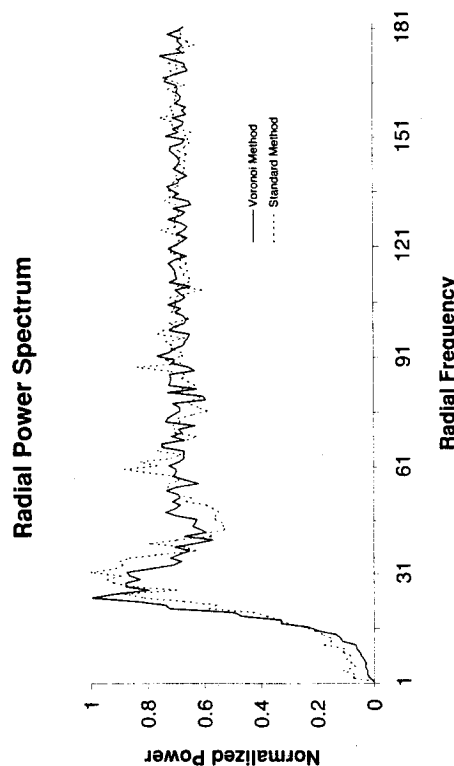


Figure 3. Radial power spectra for gray level 253. The Voronoi-based method exhibits better frequency characteristics in both low and high frequency regions, and has a sharper transition at the cutoff frequency.

fications. Dither array generation begins with an initial binary dot pattern, as before. The set of candidates for the next gray level is determined by partitioning the set of dots in the cur-

Hakan Ancin, Anoop K. Bhattacharjya, and Joseph Shu

EPSON Palo Alto Laboratory
Palo Alto, CA 94304

E-mail: Ancin.Hakan@erd.epson.com,
Bhattacharjya.Anoop@erd.epson.com,
Shu.Joseph@erd.epson.com

References

1. R. Ulichney, *The void-and-cluster method for dither array generation*, **IS&T/SPIE Symposium on Electronic Imaging**, San Jose, CA, vol. 1913, pp. 332-343, 1993.
2. T. Mitsa and K. Parker, *Digital halftoning using a blue-noise mask*, **Image Processing algorithms and Techniques, Proc. SPIE**, 1452, pp. 47-56, 1991.
3. K. Mulmuley, *Computational Geometry An Introduction Through Randomized Algorithms*, Prentice Hall, Englewood Cliffs, NJ, 1994.
4. H. Ancin, A. Bhattacharjya, and J. Shu, *Improving void-and-cluster for better halftone uniformity*, **IS&T/SPIE's Symposium on Electronic Imaging**, 24-30 January 1998.

Color filter arrays based on mutually-exclusive blue-noise patterns

Most digital still cameras use a single CCD imaging sensor to record the scene.^{1,2} Color information is encoded by means of a color filter array (CFA), which contains different color sensors placed in a regular pattern. The resulting sparsely sampled images of the three color planes are used to form a complete image by employing sophisticated interpolation algorithms. However, there are artifacts associated with sampling: aliasing. Once aliasing is introduced, even sophisticated interpolation algorithms cannot compensate for them.

The work in stochastic digital halftones provides the key to a possible solution to the problem of aliasing.³⁻⁵ Conventional halftone patterns have very regular arrays. When these patterns are scanned, the regular pattern of the halftone gives rise to aliased images. However, if one renders an image by means of any one of a number of stochastic patterns, and then images the results, the resulting image does not have the periodic, low-frequency patterns that dominate the image obtained from using the regular halftone pattern. This, despite the fact that it could be very different from the original. These results lead one to assume that the reverse should also be true. That is, if one were to capture an image with a random CFA array, the resulting image would not show the aliasing of regular, high frequency patterns in the original image.

Color filter array generation

We propose the use of blue noise masks (BNM) as the random pattern to be used to generate the random CFA.^{4,6} To generate the three-color filter arrays, one blue noise mask is multiply thresholded (with two thresholds) to obtain three mutually exclusive patterns. These patterns can then be used as the three-color filter arrays. The thresholds can be varied to adjust the number of sensors for each color filter. See figure 1 for examples of random CFAs constructed from a BNM. Blue noise masks are designed to disperse similar values evenly throughout the pattern, therefore the red, green, and blue sensor locations are more evenly distributed.

Reconstruction from CFA sampled images

The random nature of the BNM CFA makes accurate reconstruction a more challenging task. We propose a reconstruction scheme that first performs a missing-pixel edge detection to obtain edge information of the input image, and then uses an adaptive interpolation process to reconstruct the original image. See figure 2 for the flowchart of the algorithm.

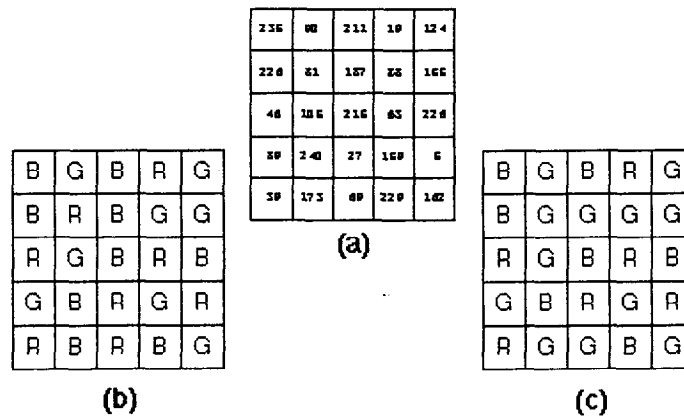


Figure 1. CFAs generated from a Blue Noise Mask. a) BNM, b) Equal number of red, green, and blue sites, c) Twice as many green sites as red or blue.



Figure 2. Flowchart of reconstruction process.

Missing Pixel Edge Detection: For vertical edge detection, we use a 3x5 or 3x7 Prewitt filter, and for horizontal edge detection, we use a 5x3 or 7x3 filter. By having longer sides, we compensate for the fact that certain pixel values are not available.

Thresholding: Since we are only interested in knowing whether or not there is an edge at a certain pixel, the edge maps can be binarized.

Morphological Opening: Because our final reconstruction step depends heavily on the accuracy of the edge detection, we perform morphological opening to the binary edge maps to remove all spurious structures that are smaller than a specified size retained from thresholding.

Reconstruction: The reconstruction process uses the edge maps obtained above to fill in all the missing pixels. This is done taking into account the directionality of the edges, and the process is identical for all three color channels.

Experimental results

We compared the performance of the BNM CFA pattern to the Bayer CFA pattern using the metric deviation from neutral, which can be used in monochrome regions to measure the performance of the CFA.² Deviation from neutral can be calculated from the RGB values for each pixel using the following equations:

$$\begin{aligned} x &= B \cos(30^\circ) - G \cos(30^\circ) \\ y &= R - B \sin(30^\circ) - G \sin(30^\circ) \\ r &= \sqrt{x^2 + y^2} \end{aligned}$$

The value of r denotes the deviation from neutral. The average value of r over all pixels can be calculated. A large average r signifies that more

pixels did not maintain their neutrality during the filtering and reconstruction process. The test images used here are horizontal stripes and vertical stripes of increasing frequency. Experimental results show that the images filtered and reconstructed using BNM CFA pattern have a smaller average deviation value than those with the Bayer CFA pattern. The output images also reflect this result. While blue and orange color banding becomes more and more obvious with increasing frequency in the reconstructed images using Bayer CFA, those images reconstructed using BNM CFA show more random color burst artifacts, but not color banding or aliasing.

We also tested our BNM CFA and the reconstruction process on natural images, and the reconstructed images showed promising results.

Due to printing constraints, the experimental images cannot be shown here in color. Please refer to Proc. SPIE 3300, paper number 28, for the test images.

Wei Zhu,** Kevin J. Parker,^a and Michael A. Kriss^b

^aDept. of Electrical Engineering
University of Rochester
Rochester, NY 14627

^bCenter for Electronic Imaging Systems
University of Rochester
Rochester, NY 14623-1212

*Current address: Eastman Kodak Company
Rochester, NY 14650-1816
Phone: 716/477-0977
Fax: 716/722-0160
E-mail: zhu@kodak.com
parker@ee.rochester.edu
mkr@troi.cc.rochester.edu

References

1. M. A. Kriss, *Electronic imaging: the challenge, the promise*. J. Soc. Photogr. Sci. Technol. 50 (5), pp. 357-378, 1987.
2. M. A. Kriss, *Color filter arrays for digital electronic still cameras*. Proc. IS&T 49th Annual Conference (Minneapolis), pp. 272-278, 1996.
3. R. A. Ulichney, *Digital Halftoning*. MIT Press, Cambridge, 1987.
4. T. Mitsa and K. J. Parker, *Digital halftoning technique using a blue-noise mask*. J.O.S.A. A 9, pp. 1920-1929, 1992.
5. R. Eschbach, Editor, *Recent progress in digital halftoning*. IS&T, Springfield, VA, 1994.
6. Q. Yu, K. J. Parker, and M. Yao, *On filter techniques for generating blue noise mask*. Proc. IS&T 50th Annual Conference, pp. 391-395, 1997.



Color conversion using neural networks

Color-coordinate conversion among a variety of color systems is crucial for color-image processing. The color conversion can be classified into two types: conversion between two color-specification systems and conversion between a color-specification system and device coordinate system. We note that the relationship between color-specification systems like CIE systems is nonlinear, and the input-output relationship of a device like color printers is usually unknown. Therefore the color conversion often requires a complicated nonlinear mapping between two color spaces.

The first type of color conversion includes color-notation conversion between the Munsell and CIE color systems. No equations have been defined for specifying a direct mapping between the two color spaces, but a table of data has been published that indicates the CIE equivalents of the Munsell notations to CIE color coordinates.¹ Therefore the conversion was carried out by three-dimensionally interpolating this table.

As for the second type, color reproduction always requires color conversion between the color signals—depending on the device used—and the standard color coordinates, representing color appearance like the CIE- $L^*a^*b^*$ color system. There are several methods for producing a desired color stimulus on a printer: an analytical method using the Neugebauer equations; matrix transformation; use of a look-up table and three-dimensional interpolation; and a neural network method.² A neural network is convenient for modeling a nonlinear transformation between two color systems for which a mathematical description is difficult. This paper describes neural network methods for the above two types of color conversion.

First we discuss the color-notation conversion between the Munsell and CIE color systems. The Munsell system is defined in three perceptual attributes of Hue, Value, and Chroma. The CIE- $L^*a^*b^*$ system is defined in the rectangular coordinates of L^* , a^* , and b^* . A mapping between one space in cylindrical coordinates (H, V, C) and another in rectangular coordinates (L^* , a^* , b^*) is realized using a multi-layer feedforward network. The conversion accuracy and speed are examined in both direc-

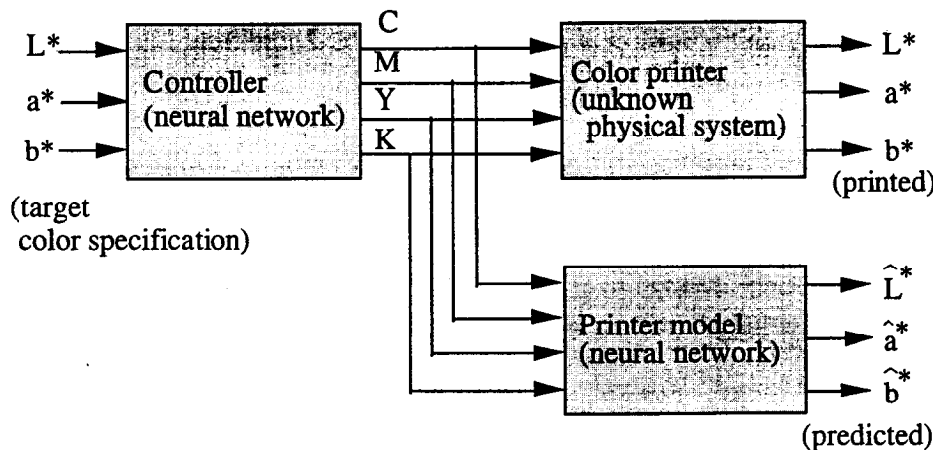


Figure 1. Color control of a printer by neural networks.

tions, Munsell-to-CIE and CIE-to-Munsell. The proposed method provides several potential advantages over the conventional approach. The direct mapping algorithm between (H, V, C) and (L^* , a^* , b^*) provides a fairly accurate conversion, compared with the indirect mapping using (X, Y, Z).³

Second we discuss a neural network method for color reproduction on a printer. Previous neural network methods were mostly considered for the control of three-color signals (CMY) of printer primaries. We need more than four inks like CMYK or CMYK plus Light Cyan and Light Magenta for high quality color reproduction. In this case, the conversion from the color stimulus values to the printer color signals is not unique. The present paper presents a solution method for realizing such a mapping problem by neural networks. We can eliminate the need to do undercolor removal (UCR) and gray component replacement (GCR).

The CIE- $L^*a^*b^*$ color system is used as the standard color space. When we regard a color printer as an unknown static system with four inputs and three outputs, the color reproduction problem is considered as the problem of controlling a system with unknown characteristics as shown in figure 1.

The color printer is an unknown physical system. A controller, which is constructed with a neural network, tries to realize the inverse mapping of the system. Therefore, the controller must determine the printer ink signals in such a way that the color stimulus errors between the targets and the printed colors are minimized. The following two-phase procedure provides a solution for this control problem.

The first phase is to identify the unknown printer system. The printer system is modeled by a neural network. The printer model is de-

termined by a learning procedure which is based on minimizing the color difference between the target $L^*a^*b^*$ values in the training data and the corresponding $L^*a^*b^*$ values predicted by the network.

The second phase is to determine a combined neural network system (combined NN system) including the controller and the printer model. We adopt an indirect approach for doing this.

The CMYK values are the internal signals of the combined NN system. From a global point of view, this combined system represents a mapping from the target $L^*a^*b^*$ values to the predicted $L^*a^*b^*$ values describing the printer outputs. Therefore, the combined NN system is trained to realize a one-to-one mapping.

When the combined NN system completes the one-to-one mapping, the network of the controller part must realize an inverse mapping of the printer model that is equivalent to the physical printer. Thus the controller can be used to determine the CMYK signals so that the desired $L^*a^*b^*$ values are produced by the printer.

The practical neural network algorithms are presented for realizing the mapping from the $L^*a^*b^*$ color space to the printer CMYK space. Moreover the method is applied to the color control using CMYK plus Light Cyan and Light Magenta. It is shown that the six-dimensional color control problem can be reduced to four-dimensional color control.

Shoji Tominaga

Osaka Electro-Communication University
Neyagawa, Osaka 572, Japan
E-mail: shoji@tmlab.osakac.ac.jp

References

1. S. M. Newhall, D. Nickerson, and D. B. Judd, *Final report of the OSA Subcommittee on spacing of the Munsell colors*, J.O.S.A. 33, pp. 385-418, 1943.
2. S. Tominaga, *A neural network approach to color reproduction in color printers*, Proc. 1st Color Imaging Conf., pp.173-177, 1993.
3. S. Tominaga, *Color notation conversion by neural networks*, Color Research and Application 18, pp. 253-259, 1993.

Insight into the solutions of the Neugebauer equations

Up until now, printer models have been inverted using iterative methods. This way, one colorant combination at most will be found to render a given color. In general, however, there may be multiple solutions for 3-ink processes, even for conventional CMY printers. In this article we show that if a color can be obtained by multiple solutions, there is a special boundary against which the solutions are laid out symmetrically. The results presented here use the Neugebauer equations for two colorants and two color values because this is easy to handle mathematically. However, all the results can be extended to the case of three colorants and three color values.

The Neugebauer equations

The Neugebauer equations¹ are considered to be the basic physical model for binary printing devices. These equations take into account both subtractive and additive color mixing. Subtractive mixing is obtained if the printed dots overlap, whereas additive mixing accounts for the additive spatial mixing of the subtractive colors. In the case of a 3-ink process, eight different colors can be obtained by subtractive mixing. Due to additive mixing of these eight colors, thousands of colors are created.

Solutions of the Neugebauer equations

The Neugebauer equations for two colorants c_1, c_2 and two color values XY can be written as:

$$X = (1-c_1)(1-c_2)X_w + c_1(1-c_2)X_1 + (1-c_1)c_2X_2 + c_1c_2X_{12}$$

$$Y = (1-c_1)(1-c_2)Y_w + c_1(1-c_2)Y_1 + (1-c_1)c_2Y_2 + c_1c_2Y_{12}$$

Each of these equations represents a hyperbola in colorant space. The asymptotes of the hyperbola are the horizontal and vertical line through its center point. Both center points and asymptotes are determined by the Neugebauer coefficients only, and do not depend on the XY values. Only the color values determine the curvature of the hyperbola. The colorant values for a given color can be obtained via a separation problem. Depending on the relative location of both hyperbolae and their respective curvatures, there can be either zero or two solutions. This is shown in figure 1: in a) there are two intersections whereas the hyperbolae do not intersect in b).

Natural gamut boundaries of the Neugebauer equations

The fact that the hyperbolae do not always intersect indicates that, for certain colors, no corresponding solution exists. This suggests that, independent of the physical restrictions (i.e. the minimum and maximum amount of colorant that can be printed), the color gamut is also limited by an additional boundary. This boundary is called the "natural boundary", as opposed to the "physical boundaries" that relate to the physical restrictions on the amounts of colorants.²

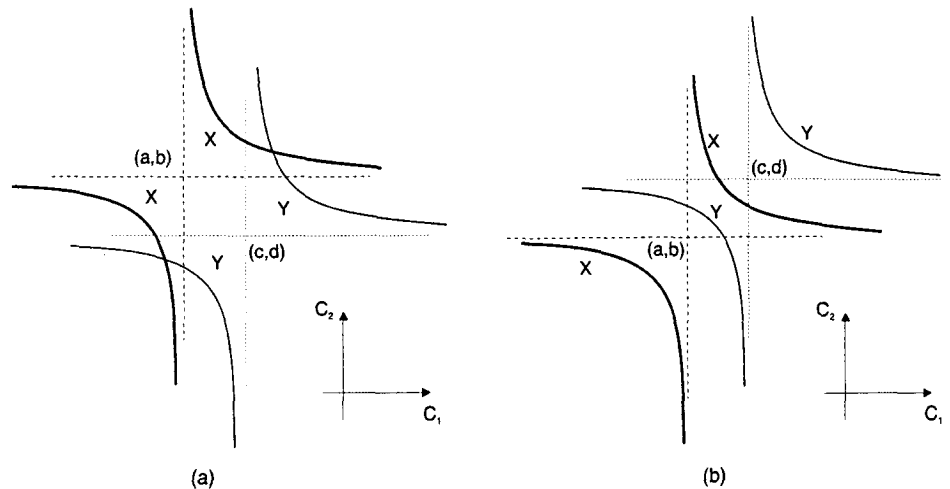


Figure 1. Two hyperbolae can have a) or not have b) intersections. Here the points (a,b) and (c,d) are the center points of the hyperbola. The dashed vertical and horizontal lines through these points are the asymptotes.

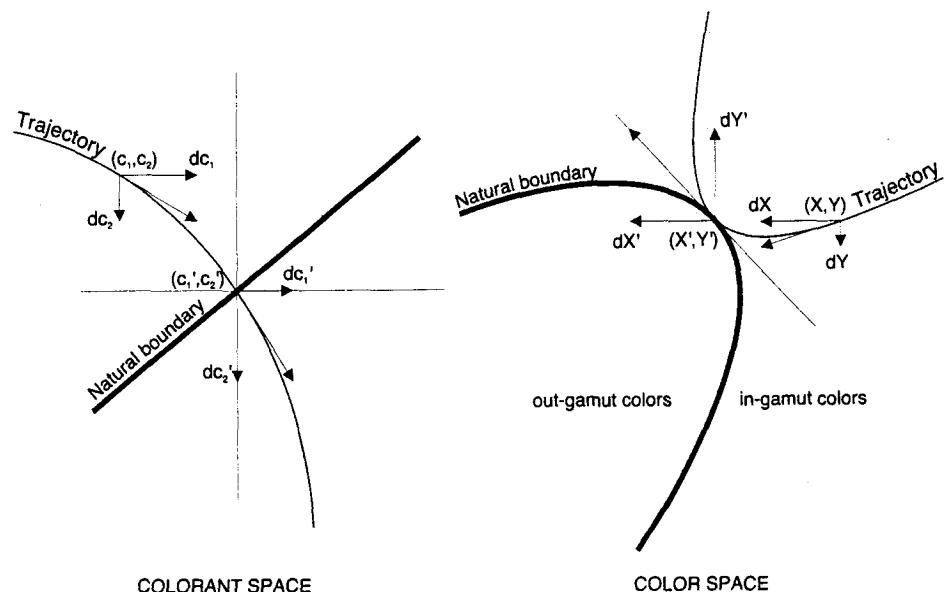


Figure 2. Natural boundary in colorant (left) and color (right) space, here referred to as gamut boundary. In this example, the color (X, Y) is an in-gamut color, whereas the color (X', Y') is a color at the gamut boundary.

Natural boundaries can be described as follows. Take a set of colorant values (c_1, c_2) that maps to a color (X, Y). A change (dc_1, dc_2) on the colorant values will result in a color change (dX, dY). The relation between both changes is expressed by the Jacobian of the Neugebauer equations.

If the determinant of the Jacobian is not equal to zero, it is possible to migrate from a color in any direction in color space and hence this color lies inside the color gamut. The situation is different if, for some colorant values, the determinant of the Jacobian is equal to zero. In that case,

it is not possible to change the color in any direction and a natural boundary point is reached.

The locus of all the points for which the determinant of the Jacobian is equal to zero is shown in figure 2 ("gamut boundary"). In colorant space, it is a line that goes through the center points of the hyperbola. In color space it is a parabola. This locus is indeed a color gamut boundary because colors on this boundary can only be changed in a direction tangential to the parabola (see "trajectory" in colorant space and

continued on p. 11

Recent research activities on data compression at the University of Toledo

In the past few years, we have been involved in the development of efficient algorithms for image and video compression. With increasing applications in video conferencing, medical imaging, telemedicine, high definition TV, multimedia, etc., efficient image and video data compression has become a necessity. A generic data compression system can be divided into three stages: representation, which is used to decorrelate the data; quantization, which is used to reduce the information into a set of reconstruction levels; and coding, to assign each quantized element a corresponding code word for transmission. Our research has been mainly concerned with the representation and quantization of both single and sequences of images. It is aimed at exploring efficient algorithms to reduce the computational complexity and bit rates while preserving the quality of the reconstructed images.

To use the advantages of both the Wavelet transform¹⁻³ and the classified vector quantizer,⁴ we have developed a novel method of classifying the Wavelet coefficients which led to an enhanced performance relative to other existing algorithms.⁵ The original image is first decomposed into a hierarchy of three layers containing ten subimages by a discrete wavelet transform. The lowest-resolution, low-frequency subimage has a relatively small size (1/64 of the original) and contains most of the energy of the wavelet coefficients. Moreover, the human visual system is more sensitive to low frequency components than to high frequency components. Therefore, the low pass subimage is simply scalar quantized and PCM coded.

This method exploits the cross correlation among the highpass subimages by combining the corresponding wavelet coefficients of the same orientation at different resolutions into vectors of different dimensions. To enhance the edge fidelity and reduce the computational complexity, classified vector quantization is used to encode the input vectors. Figure 1 shows a three-layer wavelet decomposition and the structure of vector formation.

Our classification is based on the energy of the 2×2 block in layer² and subblocks in layer 1. Horizontal subimage H_1 contains coefficients corresponding to vertical edges, patterns with significant coefficients along columns. Consequently we use the energy of the columns of the 4×4 block in H_1 as a classifying criterion for vectors of horizontal highpass subimages. Similarly, the energy of the rows of the 4×4 block in V_1 is used as a classifying criterion for vectors of vertical highpass subimages. In classifying the diagonal highpass subimages, the energy of the whole 4×4 block in D_1 is used. In

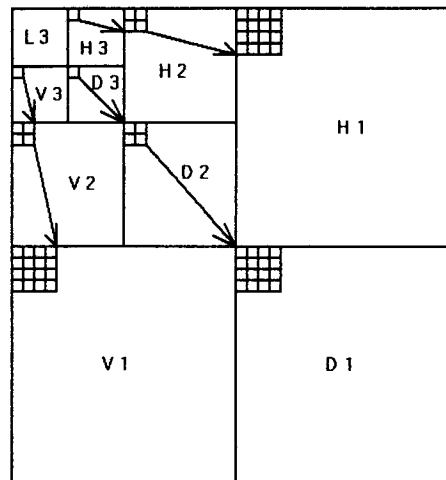


Figure 1. Structure of vector formation.

DPCM	Z^4	Z^8	Z^{16}
Z^4	Z^8	Z^{16}	D
Z^8	Z^{16}	D	D
Z^{16}	D	D	D

Figure 2. Coding strategy (D means discarded).

our scheme, vectors of horizontal and vertical subimages are classified into four classes, while vectors of diagonal subimages are classified into two. Subcodebooks are designed separately for each class by using the LBG algorithm and all high frequency subimages are vector quantized by classified-vector quantization.

A second algorithm in still-image compression exploits the simplicity of the lattice vector quantization and the efficiency of the subband coding.⁶ First, a cosine-modulated pseudo-quadrature-mirror-filter (PQMF) bank is designed to decompose the input signal into M bands. The decomposition will take place both horizontally and vertically. The PQMF significantly reduces the computational complexity and the delays associated with the subband decomposition process. The lowest frequency band is encoded by a DPCM scheme. The higher frequency bands are lattice quantized. The distribution of the higher band signals are highly non-uniform. Therefore, a piecewise uniform lattice

quantizer is used to achieve an approximately optimal VQ. With the approximate Laplacian model of the higher band coefficients, and the exceptional quantization simplicity of the cubic lattice, a pyramidal cubic lattice quantizer⁷ is adopted in this study. The vector dimension for quantization of the higher bands changes at different frequency ranges according to their energy content. Figure 2 shows the lattice quantization coding strategy used for different subbands (Z^n represents cubic lattice with dimension n). This process will lead to a high compression rate while maintaining good reconstruction quality.

An important aspect of video sequence coding is exploiting the temporal redundancy that exists between neighboring image frames. This is generally achieved by motion estimation/motion compensation techniques. One of the most popular techniques for motion estimation is the block matching algorithm (BMA). While the exhaustive search algorithm (ESA) can obtain an optimal result by searching exhaustively for the best matching block within a search window, it involves heavy computations. To reduce the computational complexity of the ESA, many fast algorithms have been developed in recent years including the three-step search⁸ widely used due to its simplicity and good performance. These algorithms often reduce the computations at the expense of the accuracy of the motion estimates. We have developed a fast algorithm for motion estimation known as the successive elimination algorithm, which achieves the same estimate accuracy as the exhaustive search with significantly reduced computational requirements.⁹ This method reduces the number of matching evaluations by considering a limited number of positions within the search window through a successive elimination process. Using an inequality constraint, many unnecessary searches for a matching block can be avoided without sacrificing the optimality of an exhaustive search.

In a follow-up effort, the concept introduced in the above fast motion estimation was expanded and applied to vector quantization.¹⁰ This work exploits the topological structure of the codebook to dynamically eliminate the code vectors in the encoding process, thus reducing the computations. A set of vectors, called control vectors, are introduced to confine the search space for the closest vector in the codebook during encoding. Each control vector provides further restrictions and constraints on the set of admissible codewords and thus progressively reduces the search space. The design is very flexible in the selection and the number of control vectors. More importantly, the scheme is a

generalization of several other existing fast vector quantization algorithms, in the sense that they can be considered as its special case.

Dr. E. Salari and S. Lin

Contact:

Dr. E. Salari

Department of Electrical Engineering and
Computer Science

The University of Toledo

Toledo, OH 43606

Phone: 419/530-8164

Fax: 419/530-8146

E-mail: esalari@uoft02.utoledo.edu

References

1. I. Daubechies, *Orthonormal bases of compactly supported wavelets*, **Commun. Pure Appl. Math.** **41**, pp. 909-996, 1988.
2. S. Mallat, *A theory for multiresolution signal decomposition: The wavelet representation*, **IEEE Trans. Pattern Anal. Mach. Intel.** **11**, pp. 674-693, 1989.
3. O. Rioul and M. Vetterli, *Wavelet and signal processing*, **IEEE Signal Proc. Mag.** **8** (4), pp. 14-38, 1991.
4. B. Ramamurthi and A. Gersho, *Classified vector quantization of images*, **IEEE Trans. Commun. COM-34** (11), pp. 1105-1115, 1986.
5. S. Lin and E. Salari, *Image Coding Using Wavelet Transform and Classified Vector Quantization*, **IEE Proc. Vision, Image and Signal Processing** **143** (5), pp. 285-291, 1996.
6. E. Salari and S. Lin, *Low Complexity Subband Image Coding with Pseudo QMF and Pyramidal Lattice VQ*, **IEE Proc. Vision, Image and Signal Processing** **144** (2), pp. 81-88, 1997.
7. T. R. Fischer, *A pyramid vector quantizer*, **IEEE Trans. Inform. Theory**, **32** (4), pp. 568-583, 1986.
8. T. Koga, K. Inuma, A. Hirano, Y. Iijima, and T. Ishiguro, *Motion Compensated Interframe Coding for Video Conferencing*, **Proc. Nat. Telecommun. Conf.**, pp. G5.3.1 - G5.3.5, 1981.
9. W. Li and E. Salari, *Successive Elimination Algorithm for Motion Estimation*, **IEEE Trans. on Image Processing** **4** (1), pp. 105-107, 1995.
10. W. Li and E. Salari, *A Fast Vector Quantization Encoding Method for Image Compression*, **IEEE Trans. Circuits and Systems for Video Technology** **5** (2), pp. 119-123, 1995.

Color FM screen design using DBS algorithm

When halftoning a color image for a four color bi-level printer, one has to obtain the halftones of the cyan, magenta, yellow, and black planes. The simplest way to do this is using a dither matrix is to threshold each color plane independently using the same matrix. This will result in halftone dots of different colors overlapping each other, thus increasing the graininess of the print. Simple schemes such as shifting the matrices have been proposed in the past to reduce graininess; but they usually reduce dot overlap at the cost of increasing other artifacts.

We propose an algorithm to jointly design a set of dither matrices such that the overall graininess is minimized. Our design goal is to achieve a uniform rendition of any printable color using cyan, magenta, yellow, and black printer dots. For example, suppose that we want to print a light gray patch with 6.25% each of cyan, magenta, yellow dots, and no black dots. If we choose to overlay the cyan, magenta, and yellow dots on top of each other, then ignoring dot gain, 6.25% of the paper will be covered by ink. The covered area will have black dots, while the uncovered area will be white paper. This results in a grainy pattern. If we disperse the cyan, magenta, and yellow dots, then a maximum of 18.75% of the paper will be covered by ink. The covered area will have either cyan, magenta, or yellow dots, while the uncovered area will be white paper. This reduces the contrast between covered and uncovered areas, resulting in a smoother pattern. To illustrate the difference, figure 1 compares a magnified image, with black dots only, to one with spatially dispersed colored dots that average to gray.

We use the direct binary search (DBS) algorithm^{1,2} to design a dither matrix for each of the primary colors of a printer. We first design an intermediate CMYK pattern. We then design all the lighter patterns by gradually remov-

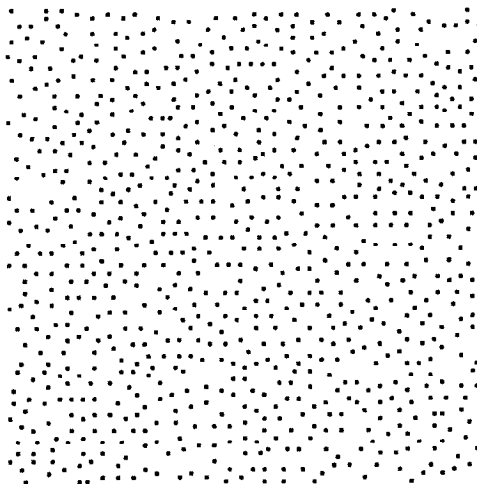


Figure 1. Magnified image showing black dots with the traditional method. Our new method uses color dots that average to gray; URL: http://www.hpl.hp.com/personal/Qian_Lin/newsletter2.html

ing dots. We next design all the darker patterns by gradually adding dots. This will ensure that the stacking property of the dither matrix is satisfied, i.e. all dots in a lighter pattern must also be present in a darker pattern.

To generate the intermediate pattern, we start with a random arrangement of a given number of cyan, magenta, yellow, and black dots. A color fluctuation function³ is defined for the halftone pattern in a uniform color space such as CIE L*a*b*. To compute the function, we apply lowpass filters that model the human visual system response to the CIE L*a*b* pixel maps, calculate the variances in the filtered pixel maps, and take a weighted sum over the color channels.

To minimize the fluctuation metric, we scan through the pixel map one pixel at a time. At each pixel, swaps are performed and the fluctuation metric is recomputed. Swapping refers

to exchanging one primary color, or white, at the current pixel with another primary color, or white, at another pixel. We select the swap, if any, that results in the largest reduction in the fluctuation metric, and keep the new pattern generated by this change. The process is continued until no swap is retained during a complete scan of the pixel map. The resulting color pattern is the intermediate pattern.

After the intermediate pattern is designed, we proceed to design the lighter and darker patterns. To design the lighter pattern, a given number of cyan, magenta, and yellow dots are deleted randomly from the intermediate pattern. We then apply the swapping operations described above. In order to satisfy the stacking property of the dither matrix patterns, only the positions of the newly deleted dots are allowed to be moved. To generate the darker patterns, a similar process is performed. The final dither matrix for each primary color is obtained by summing the binary patterns of the primary color over all gray levels.

This work was performed at the Hewlett-Packard Laboratories in Palo Alto, California

Qian Lin

Hewlett-Packard Laboratories

Palo Alto, CA, USA

E-mail: qlin@hpl.hp.com

Jan Allebach

Purdue University, West Lafayette, IN, USA

References

1. M. Anadolou and J. P. Allebach, *Model-based Halftoning by Direct Binary Search*, **Proc. SPIE** **1666**, pp. 96-108, 1992.
2. J. Allebach and Q. Lin, *FM Screen Design Using DBS Algorithm*, **Proc. IEEE Int. Conf. on Image Processing** (Lausanne, Switzerland), pp. 549-552, 1996.
3. T. J. Flohr, B. W. Kolpatzik, R. Balasubramanian, D. A. Carrara, C. A. Bouman, and J. P. Allebach, *Model Based Color Image Quantization*, **Proc. SPIE** **1913**, pp. 270-281, 1993.

Join the SPIE/IS&T Technical Group

...and receive this newsletter

This newsletter is produced twice yearly and is available only as a benefit of membership in the SPIE/IS&T Electronic Imaging Technical Group.

IS&T—The Society for Imaging Science and Technology has joined with SPIE to form a technical group structure which provides a worldwide communication network and which is advantageous to the memberships of both societies.

Join the Electronic Imaging Technical Group for US\$30. Technical Group members receive these benefits:

- *Electronic Imaging Newsletter*
- SPIE's monthly newspaper, *OE Reports*
- annual list of Electronic Imaging Technical Group members
- discounts on registration fees for IS&T and SPIE meetings and on books and other selected publications related to electronic imaging.

Persons who are already members of IS&T or SPIE are invited to join the Electronic Imaging Technical Group for the reduced member fee of US\$15.

Please Print Prof. Dr. Mr. Miss Mrs. Ms.

First (Given) Name _____ Middle Initial _____

Last (Family) Name _____

Position _____

Business Affiliation _____

Dept./Bldg./Mail Stop/etc. _____

Street Address or P.O. Box _____

City _____ State or Province _____

Zip or Postal Code _____ Country _____

Phone _____ Fax _____

E-mail _____

Technical Group Membership fee is \$30/year, or \$15/year for full SPIE and IS&T Members.

Amount enclosed for Technical Group membership \$ _____

Yes! I want to subscribe to IS&T/SPIE's *Journal of Electronic Imaging* (JEI) \$ _____
(see prices below)

Total \$ _____

Check enclosed. Payment in U.S. dollars (by draft on a U.S. bank, or international money order) is required. Do not send currency. Transfers from banks must include a copy of the transfer order.

Charge to my: VISA MasterCard American Express Diners Club Discover

Account # _____ Expiration date _____

Signature _____

(required for credit card orders)

JEI 1999 subscription rates (4 issues):	U.S.	Non-U.S.
Individual SPIE or IS&T member	\$ 40	\$ 40
Technical Group Member	\$ 60	\$ 60
Individual nonmember	\$ 80	\$100
Libraries and institutions	\$165	\$185

Your subscription begins with the first issue of the year. Subscriptions are entered on a calendar-year basis. Orders received after 1 September 1998 will begin January 1999 unless a 1998 subscription is specified.

Send this form (or photocopy) to:

SPIE • P.O. Box 10
Bellingham, WA 98227-0010 USA
Phone: (1) 360/676-3290
Fax: (1) 360/647-1445
E-mail: membership@spie.org

Please send me:

- Information about full SPIE membership
- Information about full IS&T membership
- Information about other SPIE technical groups
- FREE technical publications catalog

Electronic Imaging

The *Electronic Imaging* newsletter is published by SPIE—The International Society for Optical Engineering and IS&T—The Society for Imaging Science and Technology. The newsletter is the official publication of the International Technical Group on Electronic Imaging.

<i>Technical Group Chair</i>	Arthur Weeks
<i>Guest Editor</i>	Giordano Beretta
<i>Technical Editor</i>	Sunny Bains
<i>Managing Editor</i>	Linda DeLano
<i>Advertising Sales</i>	Mark Murgittroyd

Articles in this newsletter do not necessarily constitute endorsement or the opinions of the editors, SPIE, or IS&T. Advertising and copy are subject to acceptance by the editors.

SPIE is an international technical society dedicated to advancing engineering, scientific, and commercial applications of optical, photonic, imaging, electronic, and optoelectronic technologies.

IS&T—The Society for Imaging Science and Technology is an international nonprofit society whose goal is to keep members aware of the latest scientific and technological developments in the fields of imaging through conferences, journals and other publications.

SPIE—The International Society for Optical Engineering, P.O. Box 10, Bellingham, WA 98227-0010 USA. Phone: (1) 360/676-3290. Fax: (1) 360/647-1445. E-mail: spie@spie.org.

IS&T—The Society for Imaging Science and Technology, 7003 Kilworth Lane, Springfield, VA 22151 USA. Phone: 703/642-9090. Fax: 703/642-9094.

© 1998 SPIE. All rights reserved.

Want it published?

Submit work, information, or announcements for publication in future issues of this newsletter by e-mail to Sunny Bains at sunny@spie.org, or at the address above. Articles should be 600 to 800 words long. Please supply black and white photographs or line art when possible (figures are also accepted electronically via FTP by SPIE in TIFF and GIF formats). Permission from all copyright holders for each figure and details of any previous publication should be included. All materials are subject to approval and may be edited. Please include the name and number of someone who can answer technical questions. Calendar listings should be sent at least eight months prior to the event.



Calendar

1998

International Conference on Optical Technology and Image Processing in Fluid, Thermal, and Combustion Flow

7-9 December

Yokohama, Japan

Contact: Prof. Masaaki Kawahashi, Cochair, Saitama Univ., Dept. of Mechanical Engineering, 255 Shimo-okubo, Urawa, Saitama 338, Japan. Phone: +81 48 858 3443. Fax: +81 48 856 2577. Email: mkawa@mech.saitama-u.ac.jp/ryutai/. Web:laval.mech.saitama-u.ac.jp/vsjspie/ Cosponsored by Visualization Society of Japan and SPIE.

ICOL-98, Intl. Conf. Optics & Optoelectronics

9-12 December

Dehradun, India

Contact: Dr. O.P. Nijhawan, IRDE, Raipur, Dehradun - 248 008, India. Fax: +91 135 687161. E-mail: root@drirde.ren.nic.in

International Conference on Optics and Optoelectronics

14-18 December

Dehra Dun, India

Contact: Dr. A.K. Gupta, Instruments Research and Development Establishment, Raipur Road, Dehra Dun 248008. Phone:+91-135-687089. Fax:+91-135 687161/687128. E-mail:root@drirde.ren.nic.in. SPIE is a Cosponsor.

1999

Photonics West

23-29 January

San Jose Convention Center
San Jose, California USA

Including international symposia on

- LASE '99—High-Power Lasers and Applications
- OPTOELECTRONICS '99—Integrated Devices and Applications
- BIOS '99—International Biomedical Optics Symposium
- SPIE/IS&T's EI '99—Electronic Imaging: Science and Technology

Technical Exhibit 26-28 January

Education Program and Short Courses

For more information, contact SPIE or e-mail pw99@spie.org

Medical Imaging 1999

20-26 February

San Diego, California USA

Technical Exhibit

Instrument exhibition

SPIE Short courses

SID Symposium '99

16-21 May

San Jose, California USA

Contact: Society for Information Display, 1526 Brookhollow Dr., Ste. 82, Santa Ana, CA 92705-5421. Phone: (1) 714/545-1526. Fax: (1) 714/545-1547.

E-mail: socforinfodisplay@mcimail.com.

Web: www.sid.org

Photonics East

17-22 September

Boston, Massachusetts USA

Including international symposia on

- ISAM '99—Intelligent Systems and Advanced Manufacturing
- VVDC '99—Voice, Video, and Data Communications
- LE '99—Law Enforcement
- Industrial and Environmental Monitors and Biosensors

Abstract Due Date: 22 February

Technical Exhibit 20-22 September

Telecom '99 and Interactive '99

10-17 October

Palexpo, Geneva, Switzerland

Phone: +41-22-730-51-11. Fax: +41-22-733-72-56. E-mail: itumail@itu.int

For information about SPIE meetings, contact

SPIE, P.O. Box 10, Bellingham, WA 98227-0010 USA.

Phone: (1) 360/676-3290 • Fax: (1) 360/647-1445 • E-mail: spie@spie.org

WWW: <http://www.spie.org>

Neugebauer equations

continues from p. 7

color space in figure 2).

Location of the solutions with regard to the natural color boundary

It can be shown that the solutions to the Neugebauer equations are symmetrically laid out on a line relative to the intersection of this line with the natural colorant boundary. The slope of that line is equal to the negative of the slope of the natural colorant boundary. Hence, if one solution to the Neugebauer equations is found, the other solution can be obtained by a horizontal and vertical mirror operation (see dotted lines in figure 3).

The fact that two colorant solutions are mapped to the same color explains the paradox that the unbounded colorant space is mapped onto a bounded color space: the natural boundary divides the colorant space into two parts that are mapped onto the same region in color space. In fact the colorant space is folded along the natural colorant boundary and transformed to color space.

Marc Mahy

Agfa-Gevaert N.V.

Septestraat 27

2640 Mortsel

Belgium

Phone: +32-3-4443990

Fax: +32-3-4444240

E-mail: mmahy@eps.agfa.be

References

1. H. E. J. Neugebauer, *Die theoretischen Grundlagen des Mehrfarbenbuchdrucks*. Zeitschrift für wissenschaftliche Photographie, Photophysik und Photochemie, pp. 73-89, 1937.
2. M. Mahy, *Calculation of color gamuts based on the Neugebauer model*. Col. Res. And Appl. 22 (6), 1997.
3. M. Mahy and P. Delabastita, *Inversion of the Neugebauer equations*. Col. Res. Appl. 21 (6), 1996.

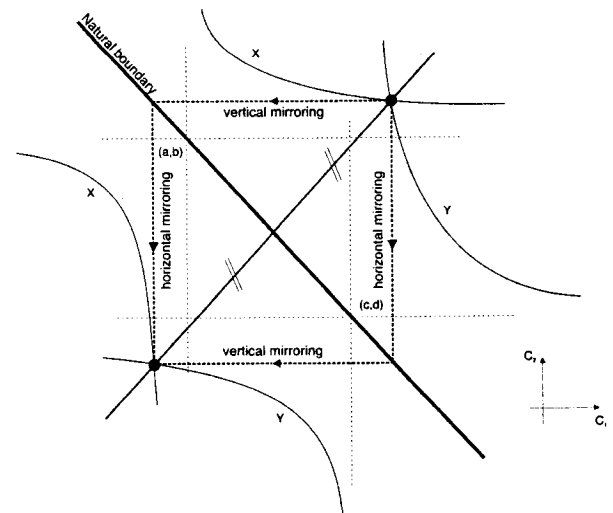


Figure 3. Location of two solutions of the Neugebauer equations.



Specifying color gamut boundaries

In addition to the characterization of all devices involved in the color reproduction process, the faithful reproduction of color images also requires the mapping of non-reproducible colors which is called "color gamut mapping". Gamut mapping needs knowledge of the exact boundary of a printer gamut represented in a color space like CIELAB.¹ Such gamuts usually have a rather complicated structure since the relationship between the device-addressing coordinates and the produced colors in the color space is strongly non-linear (figure 1). Nevertheless, it is necessary to specify the gamut boundary accurately in a form addressable by the gamut mapping algorithm.

Gamut specification

We use an approach that was designed to satisfy several demands. It should allow simple access to any arbitrary location of the gamut hull with a very compact representation. It should work with a limited number of measured reference colors (6x6x6) and produce reasonable accuracy for any desired shell location, especially the very saturated colors which occur near the corners and edges.

These demands led to the definition of a "kernel gamut" which represents the characteristics of every color gamut to contain edges and corners (figure 2), in combination with analytical functions which model the special device characteristics. The method was given the name Gamulyt which combines the terms gamut and analytical.^{2,3}

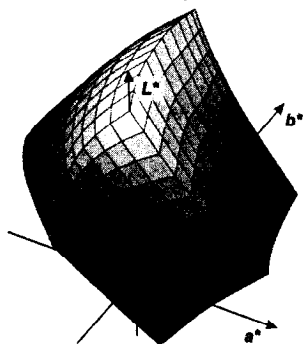


Figure 1. The color gamut of a thermal sublimation printer.

Principle of "Gamulyt"

A key feature is the introduction of cylindrical coordinates. These are very convenient in perceptual color spaces like CIELAB, CIELUV, RLAB, CIECAM etc. Using the coordinates lightness, chroma and hue-angle, it is very simple to "unwrap" the 3D color gamut around the lightness axis. This results in a representation of the form chroma plotted over lightness and hue. Figure 3 shows such a plot using CIELAB $L^*C^*h^*$. Since chroma is a function of two variables (L^* and h^*), and because this "mountain-range" has only one (folded) plane, this representation is called "two-dimensional". Reference 4 contains more information on 2D gamut plots and visualization techniques.

Gamulyt employs such a 2D representation for both the kernel and the color gamut. The kernel gamut is distorted by analytical distortion functions, which are fitted to a set of measured colors in order to reproduce the shape of the color gamut. The result is an expression for the gamut surface in the form chroma, as a function of lightness and hue-angle: $C^* = f(L^*, h^*)$.^{2,3}

Accuracy in the range of 0.8 to 1.5 CIE94 units has been reached, depending on the process considered (ink jet, thermal sublimation, offset print, photographic printer, etc.). Here, the overall number of parameters in the analytical distortion functions summed to 207.

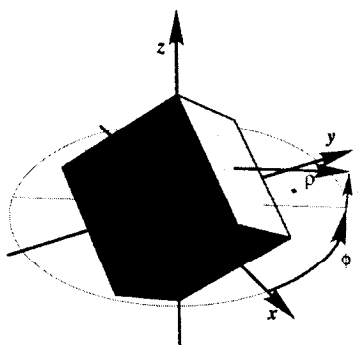


Figure 2. The kernel gamut in kernel space.

Conclusion

A new approach to specifying color gamut boundaries has been presented that has the advantages of being very compact while providing simple access to any arbitrary location of the gamut surface. The method uses the cylindrical coordinates lightness, chroma and hue of a perceptual color space. This technique has proven to be well-suited for gamut mapping¹ and to perform reasonably well.

Patrick G. Herzog

Aachen University of Technology
Department of Technical Electronics
Sommerfeldstrasse 24
52056 Aachen, Germany
E-mail: herzog@ite.rwth-aachen.de
<http://www.ite.rwth-aachen.de/herzog>

References

1. P. G. Herzog and M. Müller, *Gamut Mapping using an Analytical Color Gamut Representation*. *Proc. SPIE* 3018, pp. 117-128, 1997.
2. P. G. Herzog, *Analytical Color Gamut Representations*. *J. of Imag. Sc. & Technol.* 40 (6), pp. 516-521, 1996.
3. P. G. Herzog, *Further development of the analytical color gamut representation*. *Proc. SPIE*. 3300, pp. 118-128, 1998.
4. P. G. Herzog, *Specifying and visualising color gamut boundaries*. *Procs. of CIM '98—Color Imaging in Multimedia*, pp. 159-168, Derby, March 1998.

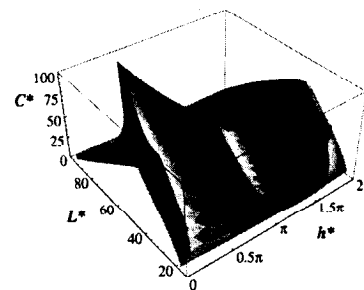


Figure 3. The color gamut in the 2D representation.

 SPIE Society of Photo-Optical Instrumentation Engineers

P.O. Box 10 • Bellingham, WA 98227-0010 USA

Change Service Requested

DATED MATERIAL

Non-Profit Org.
U.S. Postage Paid
Society of
Photo-Optical
Instrumentation
Engineers

00321523 E19-1
DR. GIORDANO B. BERETTA
HEWLETT-PACKARD CO
BLDG 3U-3 COLUMN F35
1501 PAGE MILL RD
PALO ALTO, CA 94304-1126